INTERNATIONAL JOURNAL FOR NUMERICAL METHODS IN FLUIDS, VOL. 24, 61–79 (1997)

COMPARISON OF *H* AND *P* FINITE ELEMENT APPROXIMATIONS OF THE SHALLOW WATER EQUATIONS

R. A. WALTERS

U.S. Geological Survey, 1201 Pacific Ave., Suite 600, Tacoma, WA 98402, U.S.A.

AND

E. J. BARRAGY

Intel Corporation, MS CO1-05, 15201 NW Greenbrier Pkwy., Beaverton, OR 97006, U.S.A.

SUMMARY

A *p*-type finite element scheme is introduced for the three-dimensional shallow water equations with a harmonic expansion in time. The wave continuity equation formulation is used which decouples the problem into a Helmholtz equation for surface elevation and a momentum equation for horizontal velocity. An exploration of the applicability of *p* methods to this form of the shallow water problem is presented, with a consideration of the problem of continuity errors. The convergence rates and relative computational efficiency between *h*- and *p*-type methods are compared with the use of three test cases representing various degrees of difficulty. A channel test case establishes convergence rates, a continental shelf test case examines a problem with accuracy difficulties at the shelf break, and a field-scale test case examines problems with highly irregular grids. For the irregular grids, adaptive *h* combined with uniform *p* refinement was necessary to retain high convergence rates.

KEY WORDS: finite element; shallow water equations; adaptive refinement; convergence

1. INTRODUCTION

The shallow water equations are a non-linear, coupled set of equations for surface elevation and velocity that have wide application in hydrology, oceanography and meteorology. Several computational forms of these equations have been explored in the literature, one of the most effective of which is the wave continuity equation formulation.[1–12] This form of the equations has been studied in the context of both time-stepping and harmonic expansion schemes. Among its many advantages are computational efficiency, freedom from grid-scale noise and a demonstrated robustness on field-scale problems.

However, this formulation does not preserve local continuity exactly and in fact significant errors can arise.[13] As a practical matter, continuity errors can be used as a quantitative measure of accuracy. The result is that with this formulation there is a requirement for an accurate surface elevation solution so as to maintain continuity accuracy. As noted from another study,[14,15] quadratic elements seem to give considerably more accurate results than linear elements for the wave equation form of the shallow water equations, although the increased accuracy in velocity is not so pronounced. These

CCC 0271–2091/97/010061–19

Received 11 January 1995
Revised 15 April 1996

results suggest the application of *p*-type finite elements to the shallow water equations as an alternative to *h* refinement, particularly for the wave equation formulation.

The *h* finite element method achieves convergence of the approximate solution by refining the element mesh, parametrized by the mesh size *h*.[16] In contrast, the *p* method achieves convergence by refining the degree of the polynomial approximation within each element while the element mesh spacing *h* is held fixed. Discussions of the method and its theoretical convergence properties can be found in References 17–19. These methods and the closely related spectral element method have been applied successfully to several types of fluid problems.[20–26] Comparatively little work has been done in applying *p* discretizations to the shallow water problem.[15,27,28] For problems with sufficient smoothness, *p* methods may offer much higher rates of convergence and hence may lead to significant computational advantages. Given that they may provide substantially more accuracy than an *h* method for similar computational expense suggests that *p* methods may be particularly appropriate in the present shallow water formulation, where accuracy in the surface elevation is necessary to maintain continuity accuracy.

Our purpose in this study is to explore the applicability of *p*-type finite elements to the wave equation formulation of the shallow water equations. A preliminary comparison of an *h*-type method with a *p*-type method is presented. Studies of both relative error and computational efficiency are presented. In the following sections we first develop the mathematical and numerical models that are used in the analysis. Following this, computational results for three test cases with different degrees of difficulty are presented.

2. MATHEMATICAL MODEL

Sea level (surface elevation) and velocity may be calculated with a finite element model that solves the three-dimensional shallow water equations with the conventional hydrostatic assumption and Boussinesq approximation and eddy viscosity closure in the vertical. The development of the equations is outlined briefly here; for more details see References 2, 3, 6 and 9. The shallow water equations consist of the continuity equation

$$\nabla \cdot \mathbf{u} + \frac{\partial w}{\partial z} = 0, \tag{1}$$

its two-dimensional vertical average

$$\frac{\partial \eta}{\partial t} + \nabla \cdot (h + \eta)\bar{\mathbf{u}} = 0 \tag{2}$$

and the horizontal components of the three-dimensional momentum equation

$$\frac{\partial \mathbf{u}}{\partial t} + \nabla \cdot (\mathbf{u}\mathbf{u}) + \mathbf{f} \times \mathbf{u} + g\nabla\eta - \frac{\partial}{\partial z}\left(A_{\mathrm{v}} \frac{\partial \mathbf{u}}{\partial z}\right) = \mathbf{F}, \tag{3}$$

where horizontal friction has been neglected, surface and bottom boundary conditions are given as

$$A_{\mathrm{v}} \frac{\partial \mathbf{u}}{\partial z} = \frac{\tau_{\mathrm{s}}}{\rho} \quad (z = \eta), \tag{4}$$

$$A_{\mathrm{v}} \frac{\partial \mathbf{u}}{\partial z} = \frac{\tau_{\mathrm{b}}}{\rho} = C_{\mathrm{D}}|\mathbf{u}|\mathbf{u} \quad (z = -h), \tag{5}$$

essential boundary conditions on η are set at open boundaries and $\mathbf{u} \cdot \bar{\mathbf{n}} = 0$ (no normal flow) on land boundaries.

The various terms appearing in these equations are defined as follows. The surface elevation relative to mean sea level is given as $\eta(x, y, t)$, $\mathbf{u}(x, y, z, t)$ is the horizontal velocity and $w(x, y, z, t)$ is the vertical velocity; $\bar{\mathbf{u}}(x, y, t)$ is the vertical or depth average of $\mathbf{u}$. The water depth from mean sea level is given as $h(x, y)$, while $H(x, y)$ is the total water depth such that $H = h + \eta$; $\mathbf{f}$ is the Coriolis vector and g is gravitational acceleration. The surface stress is denoted as τ_S and τ_b denotes the bottom stress; C_D is the bottom drag coefficient and ρ is the reference density. $A_v(x, y, z, t)$ is the vertical eddy viscosity, $\mathbf{F}$ represents body forces such as density gradient forces and ∇ is the horizontal gradient operator $(\partial/\partial x, \partial/\partial y)$. The vertical eddy viscosity can be defined in several ways depending on the extent to which the bottom boundary layer is to be resolved. A general form used in this analysis is

$$A_v(x, y, z, t) = A_0|\mathbf{u}_b|H\left((1 - R)\frac{z + H}{0{\cdot}2H} + R\right), \quad -H \leqslant z \leqslant -0{\cdot}8H, \tag{6}$$

$$A_v(x, y, z, t) = A_0|\mathbf{u}_b|H, \quad z \geqslant = -0{\cdot}8H, \tag{7}$$

where $\mathbf{u}_b(x, y, t)$ is the bottom velocity, A_0 is a scaling factor and R is the ratio between minimum and maximum viscosity in the vertical.

The present work employs a harmonic decomposition in time rather than using discrete time-stepping methods.[1,6,8] Thus it is applicable to a wide range of problems that use steady or periodic forcing, such as astronomical and radiational tides and steady flows. This approach leads to greatly enhanced efficiency and allows exploratory studies of complicated problems. The harmonic decomposition procedure can be briefly described as follows. At the outset the dependent variables are expressed as periodic functions of a relatively small number of frequencies or tidal constituents,

$$\eta(x, y, t) = \tfrac{1}{2}\sum_{n=-N}^{N} \eta_n(x, y)\mathrm{e}^{-i\omega_n t}, \tag{8}$$

$$\mathbf{u}(x, y, z, t) = \tfrac{1}{2}\sum_{n=-N}^{N} \mathbf{u}_n(x, y, z)\mathrm{e}^{-\mathrm{i}\omega_n t}, \tag{9}$$

where ω is the angular frequency and n is the index for the N tidal and residual constituents. Applying (8) and (9) to (2) and (3) and extracting the frequency ω_n,[2] the governing equations become

$$-\mathrm{i}\omega_n\eta_n + \nabla\cdot(h\bar{\mathbf{u}}_n) = \nabla\cdot\mathbf{W}_n, \tag{10}$$

$$-\mathrm{i}\omega_n\mathbf{u}_n + \mathbf{f}\times\mathbf{u}_n - \frac{\partial}{\partial z}\left(A_v\frac{\partial\mathbf{u}_n}{\partial z}\right) = -g(\nabla\eta_n - \mathbf{T}_n), \tag{11}$$

where $\mathbf{W}_n$ contains the non-linear terms arising in the harmonic form of the continuity equation and $\mathbf{T}_n$ contain both the density-forcing term and all the non-linear terms in the harmonic form of the momentum equation. These include both advection and terms arising from time-dependent viscosity.[9,29] The treatment of $\mathbf{W}_n$ and the advection terms in $\mathbf{T}_n$ is straightforward as they contain

only simple products of the various frequencies appearing in the harmonic expansion. Thus they lead to sums and differences between the frequencies of the N constituents and contribute as source terms in the generation of overtides, compound tides and low-frequency tides.

$$\mathbf{W}_n = -\tfrac{1}{2} \sum_{i,j=-N}^{N} \eta_i \bar{\mathbf{u}}_j, \quad \omega_i + \omega_j = \omega_n, \tag{12}$$

$$\mathbf{T}_n = -\frac{1}{2g} \sum_{i,j=-N}^{N} \nabla \cdot (\mathbf{u}_i \mathbf{u}_j) - \frac{1}{\rho} \int_z^{\eta} \nabla(\delta\rho)\, \mathrm{d}z' + \mathbf{T}_{\mathrm{A}}, \quad \omega_i + \omega_j = \omega_n. \tag{13}$$

The first term in $\mathbf{T}_n$ is the advective component, also known as the tidal stress, the second term is the baroclinic forcing due to horizontal density gradients, where $\delta\rho$ is the density anomaly, and the third term arises from the time dependence of A_{v},[29] which vanishes in this study because A_{v} is taken as constant in time. The treatment of the vertical friction term $\mathbf{T}_{\mathrm{A}}$ and bottom friction term can present additional difficulties as they generally contain a factor $|\mathbf{u}|$. These terms are approximated by expanding in a Taylor series about the time-independent part of $|\mathbf{u}|$. The technique is an extension of the approach developed in Reference 2 for the two-dimensional, shallow water equations in a finite difference context to three dimensions and the finite element method.[9,29]

In a primitive equation model with harmonic decomposition in time, equations (10) and (11) are used as the governing equations and discretized directly. This approach suffers from a number of problems in both the harmonic decomposition form and the time-stepping form, such as spurious modes and problems with the propagation of grid-scale waves.[3,14] An alternative form of the continuity equation, referred to as the wave continuity equation, is used here. Details of the derivation and studies of the method can be found in References 2–4 and 6–9. One obtains for the continuity equation a Helmholtz problem.

$$-\mathrm{i}\omega_n \eta_n - \nabla \cdot \left(\frac{gh}{q_n^2 + f^2} [q_n(\nabla\eta_n - \bar{\mathbf{T}}_n) - \mathbf{f} \times (\nabla\eta_n - \bar{\mathbf{T}}_n)] \right) = \nabla \cdot \mathbf{W}_n, \tag{14}$$

where $q_n = \mathrm{i}\omega_n + \gamma$, with $\gamma(x, y)$ being the time-independent part of bottom friction, and $\bar{\mathbf{T}}_n$ is the depth average of $\mathbf{T}_n$ with the inclusion of surface stress and the time-dependent part of bottom stress. This form of the equation has the additional advantage that the solution for sea level and the solution for velocity are decoupled, leading to greater computational efficiency. In practice a matrix equation for sea level is solved first, followed by a solution for velocity that uses these sea level values. This procedure is iterated until convergence (typically 5–10 iterations per constituent).

3. NUMERICAL MODEL

This study focuses on the solution for surface elevation in the two-dimensional, depth-averaged wave equation form of the continuity equation (14) and the solution for horizontal velocity components in the three-dimensional momentum equation (11). These governing equations are approximated using standard Galerkin techniques. A Lagrange basis is used for all the variables. The equation for sea level is discretized by defining a set of two-dimensional triangular elements in the horizontal plane. As mentioned above, a standard Lagrange basis of polynomial degree p is defined on the master element.[16] The momentum equation for velocities is discretized by defining a set of three-dimensional prismatic elements. These elements are constructed from the 2D elements used for the wave continuity equation by simply extending them prismatically in the vertical direction, over which a piecewise linear expansion is used. With the elements defined in this way, it is convenient to express the basis functions as a tensor product of the horizontal bases and the vertical bases, i.e.

$\Phi = \phi(x, y)\zeta(z)$.[6,7,9] The vertical co-ordinates are terrain-following co-ordinates or -co-ordinates so that there are a fixed number of nodes in the vertical beneath each surface node. There are well-known problems with this non-orthogonal co-ordinate system.[10,30] However, none of the test cases presented here suffers from these difficulties.

The continuity equation (14) can be expressed in weighted residual form as: find $\eta \in H$ such that

$$-\mathrm{i}\omega_n \int_\Omega \hat{\eta}\eta_n \, \mathrm{d}\Omega + \int_\Omega \nabla\hat{\eta} \cdot \{\alpha[q_n(\nabla\eta_n - \bar{\mathbf{T}}_n) - \mathbf{f} \times (\nabla\eta_n - \bar{\mathbf{T}}_n)] - \mathbf{W}_n\} \, \mathrm{d}\Omega = -\oint \mathbf{Q}_n \cdot \mathbf{n} \, \mathrm{d}\Gamma \quad \forall\hat{\eta} \in H, \tag{15}$$

where $\alpha = gh/(q_n^2 + f^2)$ and the divergence term has been integrated by parts. Here is the volume of the domain and Γ is the boundary. The terms $\mathbf{W}_n$ and $\bar{\mathbf{T}}_n$ are treated as data and $\mathbf{Q}_n = H\mathbf{u}_n$. Expanding η_n and $\hat{\eta}$ in terms of the finite element basis and numerically integrating produces a linear algebraic problem for the nodal unknowns.

The weak form of the momentum equation can be given as: find $\mathbf{u}_n \in H \times H$ such that

$$-\mathrm{i}\omega_n \int_\Omega \hat{\mathbf{u}}\mathbf{n}_n \, \mathrm{d}\Omega + \int_\Omega \hat{\mathbf{u}}(\mathbf{f} \times \mathbf{u}_n) \, \mathrm{d}\Omega - \int_\Omega \frac{\partial\hat{\mathbf{u}}}{\partial z} \cdot A_\nu \frac{\partial\mathbf{u}_n}{\partial z} \, \mathrm{d}\Omega = -g \int_\Omega \hat{\mathbf{u}}(\nabla\eta_n - \mathbf{T}_n) \, \mathrm{d}\Omega \quad \forall\hat{\mathbf{u}} \in H, \tag{16}$$

where the equation is interpreted componentwise. Expanding $\mathbf{u}_n$ and $\hat{\mathbf{u}}$ in terms of the finite element basis again produces a linear algebraic problem for the nodal unknowns. Normally this would produce a fully 3D problem. However, owing to the tensor product nature of the basis Φ, it is possible to obtain a much simpler problem. This is done by applying node point integration in the horizontal and analytic integration (with linear bases) in the vertical. This effectively diagonalizes the matrix problem in the horizontal and leaves one with a tridiagonal system in the vertical for each surface node in the problem. This method is known as integral lumping[6,7] and is related to mass lumping for time-stepping schemes. This method gives acceptable errors in velocity, which is dominated by errors in surface elevation gradient.

4. RESULTS AND DISCUSSION

Three test cases were examined: a tidally forced channel that is used to demonstrate convergence, a shelf problem with density forcing that is used to investigate problems with continuity errors and compare computational efficiencies, and a field-scale problem with highly irregular geometry that is used to investigate issues of irregular domains and computational efficiency.

4.1. Channel problem

This test case is a rectangular channel with tidal forcing at one end, solid boundaries on the other three sides and a water depth that varies linearly from the open boundary to the opposite end. This problem has an analytical solution which is used to calculate the L^2 norm of the error. (Details can be found in Reference 13, p. 191, with 1 m km^{-1} bottom slope.) The model parameters in (14) are $\mathbf{f} = 0, \gamma = 0, \mathbf{T}_n = 0$ and $\mathbf{W}_n = 0$ and the solution is given by

$$\eta = [AJ_0(2(kx)^{1/2}) + BY_0(2(kx)^{1/2})]\cos(\omega t), \tag{17}$$

$$u = -\left(\frac{g}{S_0 x}\right)^{1/2} [AJ_1(2(kx)^{1/2}) + BY_1(2(kx)^{1/2})]\sin(\omega t), \tag{18}$$

a linear, inviscid standing wave with $u = 0$ at $x = x_0, \eta = a\cos(\omega t)$ at $x = x_1$ and $H = S_0 x$ for $x_0 \leqslant x \leqslant x_1$, where $A = aY_1(2(kx_0)^{1/2})/D, B = -aJ_1(2(kx_0)^{1/2})/D$, $D = Y_1(2(kx_0)^{1/2})J_0(2(kx_1)^{1/2}) - Y_0(2(kx_1)^{1/2})J_1(2(kx_0)^{1/2})$, $k = \omega^2/S_0 g, x_1 = 10{,}000$ m, $x_0 = x_1 - 4000$ m, $S_0 = \mathrm{d}H/\mathrm{d}x = 0{\cdot}001$ and J and Y are Bessel functions of the first and second kind respectively.

This problem is used to demonstrate convergence rates for uniform h and p refinement of the same initial grid. This initial grid had six nodes: two nodes across the channel and three nodes along the channel. For the h-type convergence study this grid was uniformly refined, producing a sequence of grids with 3×2,5×3,9×5,17×9 and 33×17 nodes. The p refinement study was based on the initial 3×2 node grid, which had four elements. This element grid was run with values of $p = 1, 2, 3, 4, 6$ and 8, where p is the degree of the polynomial approximation within the element. For $p = 1, 2, 4$ and 8 the p grids have an h refinement counterpart with an identical number of nodes and identical node placement. These two sequences of calculations give a comparison between h and p refinement for identical nodal grids. All models and analytical solution calculations were done in double precision.

The results for the h refinement ($p = 1$ linear element) are shown in Table I, which also shows the number of nodes in the mesh, N, the uniform refinement level R, the rate of convergence for the L^2 error in the sea level η and the rate of convergence for the L^2 error in the velocity u. The rate for refinement level R is computed using the L^2 errors at mesh refinements R and $R - 1$. As indicated in the table, the sea level solution converges at a rate of $O(h^2)$ as expected, while the velocity solution converges at a rate of $O(h^{3/2})$.

A comparison of h and p convergence rates is shown in Figure 1. This figure shows the variation in the L^2 norm of the sea level and velocity errors as the number of degrees of freedom in the mesh varies. The two upper lines in the figure show the h convergence results of Table I with $p = 1$. The two lower lines show the p convergence results which are consistent with the expected rates[19] of $O(h_0^{p+1})$, where h_0 is the element mesh spacing of the grid and p is the degree of the polynomial approximation. These results indicate the dramatic convergence rates that can be obtained with p refinement. The limits of accuracy for the p refinement are reached at an error level of about 10^{-9}. It was verified that this was due to round-off error within the code.

4.2. Shelf problem

The continental shelf problem has two cases. Both represent an idealized shelf with a horizontal density gradient normal to the depth contours. The first case contains a shelf in the left half of the domain, a shelf break at the midpoint and a steep slope in the right half of the spatial domain which is a square measuring 50 km on a side (Figure 2). The depth varies linearly in both the left and right

Table I. Rectangular channel: rate of convergence in sea level η and velocity u as mesh is refined for linear elements (N, number of nodes; R, refinement factor)

N	R	η	u
6	0	1·848	1·477
15	1	1·848	1·477
45	2	1·926	1·517
153	3	1·982	1·485
561	4	1·900	1·604

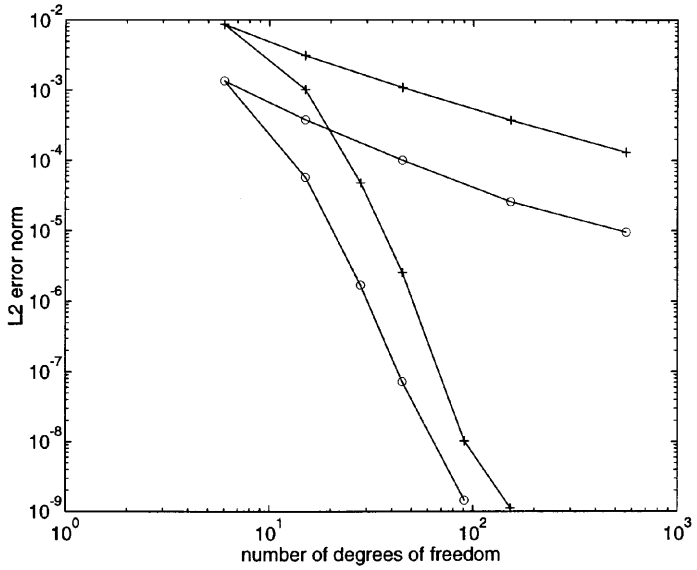

Figure 1. Rectangular channel: variation in L^2 error in sea level (○) and velocity (+) as mesh size varies

halves of the domain, with a variation from 10 to 100 m in the left half and from 100 to 600 m in the right half. The domain is 50 km × 50 km. In previous studies, accuracy problems have occurred at the discontinuity in bottom slope at the shelf break. For this case the model parameters are $\mathbf{f} = 0, \mathbf{u} = \mathbf{0}$ at the bottom, $\mathbf{W}_n = 0$ and $\mathbf{T}_n$ contains a pressure gradient force from a horizontal density gradient. The density gradient is constant across the domain so that $\mathbf{T}_n$ is proportional to the depth, which is then a piecewise linear function. An analytical solution is available for the vertical profile of velocity and the depth-averaged velocity is zero everywhere.

$$u = \frac{1}{48}\frac{g\lambda h^3}{\rho A_{\mathrm{v}}}(8\xi^3 - 9\xi^2 + 1), \tag{19}$$

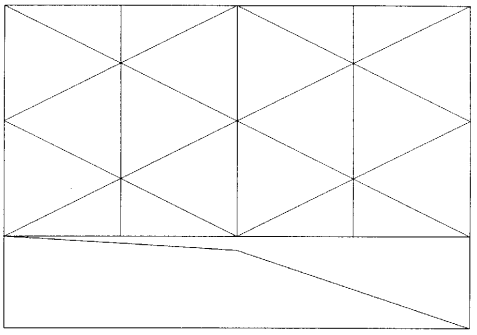

Figure 2. Grid for shelf break test case with bathymetry shown along transect

where $\lambda = \partial\rho/\partial x$ and $\xi = -z/h$ such that $\xi = 0$ at the surface and $\xi = 1$ at the bottom. Details of the boundary conditions and derivation of the analytic solution can be found in References 10 and 31. For the parameters used here,

$$u = 0{\cdot}1274(8\xi^3 - 9\xi^2 + 1). \tag{20}$$

Taking $A_v/h^3 = \text{constant} = 5 \times 10^{-8}$ this equation holds at any point in the horizontal plane.

This problem, with piecewise linear bathymetry, appears deceptively simple. In fact, for the formulation considered here, it can display severe accuracy problems in the velocity at the shelf break. For linear elements with *h*-type refinement it is observed that the depth-averaged velocity is not very accurate over a sequence of mesh refinements, but it does converge. Table II shows the L^2 norm of the sea level error and depth-averaged velocity for the case of linear elements. The sequence of meshes used here is identical with that used for the rectangular channel case; 21 equispaced levels were used in the vertical. The error in sea level stagnates at slightly below 0·00194 because of insufficient resolution in the vertical (which prevents an accurate resolution of the bottom friction).

More interesting are the results obtained for quadratic elements, where the solution of velocity is very accurate (at round-off) even for the coarsest element mesh. This behaviour can be explained by examining equation (15). Note that for $\mathbf{f} = 0, \omega_n = 0, \mathbf{W}_n = 0$ and $\mathbf{Q}_n = 0$ one obtains

$$\nabla\hat{\eta} \cdot \left(\frac{gh}{q_n^2 + f^2} q_n (\nabla\eta_n - \mathbf{T}_n) \right) = 0 \quad \forall\hat{\eta} \in H \tag{21}$$

for the wave equation and a term $\nabla_\eta n - \mathbf{T}_n$ appears in the momentum equation. This may be interpreted as requiring $\nabla\eta_n = \mathbf{T}_n$ in some weighted residual sense. For this test case, $\mathbf{T}_n$ varies piecewise linearly within the domain owing to the bathymetry. Using linear triangular elements to approximate η_n implies that $\nabla\eta_n$, a piecewise constant function, is to approximate a piecewise linear function in some weighted residual sense. The results are understandably bad because the polynomial orders are different. However, using quadratic triangular elements to approximate the sea level implies that a piecewise linear function is to match the piecewise linear variation in $\mathbf{T}_n$. This gives essentially exact results.

The vertical velocity profiles have definite characteristics that point to the source of error. The velocity is composed of a barotropic mode, whose vertical profile appears as a typical boundary layer profile and is driven by the surface pressure gradient force, and a baroclinic mode, whose vertical profile is given by (19) and is driven by the internal pressure gradient force due to the horizontal density gradient. The test problem is designed so that the barotropic mode vanishes. In a previous study it was found that the baroclinic mode converged at a rate of $O(\Delta z^2)$ as is expected for linear elements in the vertical.[10] In this study it was found that the errors are dominated by contributions from the barotropic mode. This indicates that the velocity errors, and hence continuity errors, are

Table II. Shelf break piecewise linear bathymetry: L^2 error in sea level η and velocity u as mesh is refined for linear elements (N, number of nodes; R, refinement level)

N	R	$L^2\eta$	L^2u
6	0	0·01947	1·594
15	1	0·00532	0·520
45	2	0·00237	0·184
153	3	0·00194	0·065

dominated by errors in sea level gradient arising from errors in the solution of (14). The results for this problem and examination of equation (21) indicate that sea level errors may be exacerbated when equal-order interpolation is used for η and $\mathbf{u}$. These problems and some implications for p refinement are explored further with a variation of this test case as described next.

The second case of the shelf break problem has bathymetry that varies as a hyperbolic tangent function (Figure 3). The domain is 100 km across-shelf by 50 km along-shelf. The bathymetry is given as $h = a + b\tanh[k(x - x_c)]$, with $a = 505, b = 495/\tanh(kx_c), k = 0{\cdot}1$ km and $x_c = 50$ km, which gives a depth of 10 m at the shoreline boundary and 1 km at the ocean boundary at $x = 100$ km. Varying the parameter k allows a transition from a problem with essentially linear variation in bathymetry to one with a sharp shelf break at the middle of the domain. In this test case, k has been chosen such that the width of the shelf break is roughly 10 km. An analytic solution can be derived as in the previous problem with piecewise linear bathymetry and used to compute L^2 errors.

This problem provides more interesting comparison than the case of piecewise linear bathymetry. Here again the sequence of meshes employed for the rectangular channel problem has been used, with 41 levels in the vertical. The finest mesh is shown in Figure 3. Within each element the depth data are interpolated to the same degree as the polynomial approximation for sea level. Thus this problem has the property that as the grid is refined, the bathymetry data are resolved to increasingly greater accuracy. For the coarsest mesh with linear elements the bathymetry appears to vary linearly across the domain. As the mesh is refined, the hyperbolic tangent variation in depth across the domain is eventually resolved.

Table III shows the L^2 norm of the sea level error and depth-averaged velocity, as well as the maximum frontal solver frontwidth and frontal solution time for a discretization of linear elements. Recall that for this problem the depth-averaged velocity of the true solution is zero. Therefore the norm of the depth-averaged velocity may be interpreted as an error norm. Note that for the coarsest meshes the errors are quite bad as would be expected from the experiences with the piecewise linear shelf break problem. Note also that at the mesh is refined, the bathymetry data are refined and approach the hyperbolic tangent function. Examining the L^2 norm of the error in the depth-averaged velocity for the three finest meshes shows that the velocities are converging at a rate of $O(h^2)$ as expected. The error in sea level beings to stagnate for the most refined grid, again owing to insufficient resolution of the bottom boundary layer.

Figure 4 shows the L^2 norm of the error in the depth-averaged velocity as the number of degrees of freedom is varied. The figure shows standard h convergence results for linear elements (uniform $h, p = 1$ curve), as taken from Table III above. Also shown are p convergence results for four different element meshes, labelled $R = 0, 1, 2, 3$. These four base element meshes correspond to the

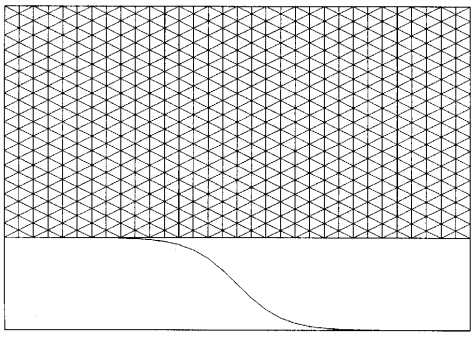

Figure 3. Grid for shelf break test case with tanh bathymetry shown along transect

Table III. Shelf break hyperbolic tangent bathymetry: results as mesh is refined for linear elements (N, number of nodes; R, refinement level; FW, frontwidth; t_{solve}, frontal solve time)

N	R	$L^2\eta$	L^2u	FW	t_{solve}
8	0	0·0760843	7·61813	3	0·12
17	1	0·0216523	2·28807	5	0·19
49	2	0·0053078	0·34924	7	0·40
161	3	0·0012858	0·08577	13	1·25
577	4	0·0002798	0·02123	25	5·05
2209	5	0·0001373	0·00561	50	27·43

four coarsest meshes generated in the h convergence study. Note that the p refinement generates exponential convergence in terms of the number of degrees of freedom, as indicated by the increasing slope of the error curves as p is increased. Here again the dramatic effects of p convergence are illustrated.

However, the results are complicated by the fact that the bathymetry must be fully resolved before the high convergence rates can be obtained. In this case, note the anomalous behaviour in convergence in the range of 100 to 300 degrees of freedom. This is the range where the bathymetry becomes fully resolved. Above this range the bathymetry variation is well resolved and high convergence rates are obtained. Recall that the bathymetry data are interpolated within each element by a polynomial of the same degree as that used to approximate the sea level. In the range of 100 to 300 degrees of freedom, for sufficiently high p, the interpolant of the bathymetry data exhibits

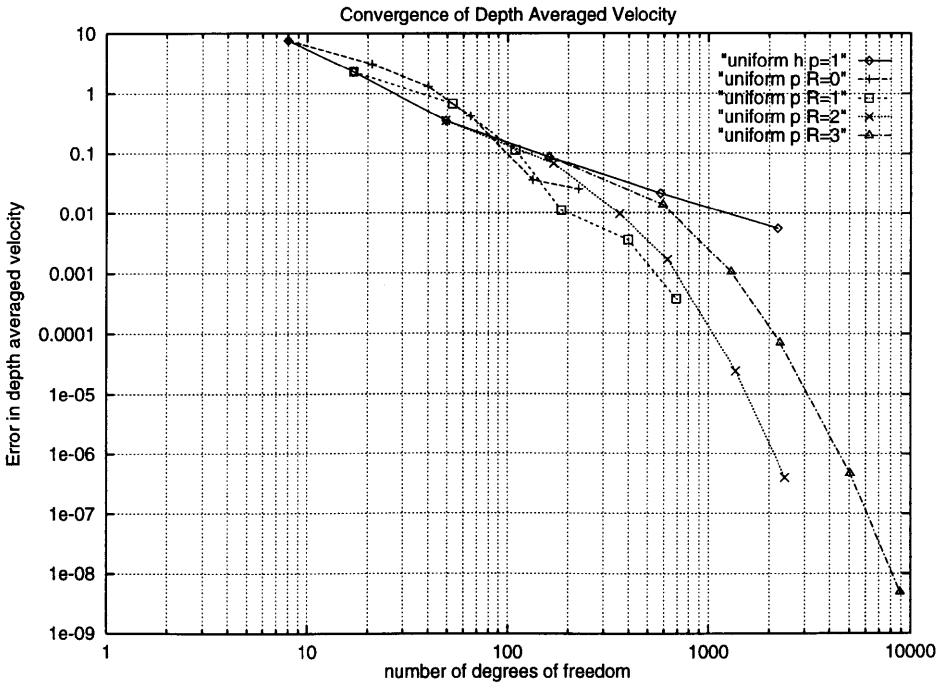

Figure 4. Shelf break hyperbolic tangent bathymetry: variation in L^2 error in depth-averaged velocity for h and p refinement. Uniform h refinement of grid $R = 0$ generated the grids $R = 1, 2, 3$ are that listed in Table III

oscillatory behaviour near the shelf break. Thus in the figure one sees good convergence as p increases for the $R = 0$ mesh until $p \geqslant 6$ is reached. At this point, oscillations in the bathymetry data develop and there is a kink in the convergence plot. Similar results are observed for the $R = 1$ mesh. For $R = 2$ and 3 the initial element mesh is sufficiently refined to avoid this phenomenon for the particular tanh variation chosen and range of p.

Also of interest are the observed sea level solution times for the frontal solver for different combinations of h and p. Table IV shows the refinement level R, the L^2 norm of the error in the depth-averaged velocity and the solution time in seconds for varying values of p. These values are plotted in Figure 5. These results must be interpreted with some care. They reflect the frontal solution time (including forming the elements) for non-optimized code running on an RS6000 workstation. No modifications to the frontal solver have been made to take advantage of the special structure of p-type discretizations. Instead, the timings give a reasonable reflection of the flop count associated with each discretization.

A comparison of the efficiency of h and p refinement is given by specific data points in Table IV: $R = 5, p = 1$; $R = 2, p = 4$ and $R = 1, p = 6$ show similar error levels but a decrease in the solution time by a factor of six for the high-p cases. The disparity is greater as the norm of the error drops. For example, at an error level of 10^{-4} one can compare the $R = 5, p = 3$ and $R = 2, p = 6$ solutions. The disparity in the run times is greater than a factor of 20. An alternative way of examining the results in Table IV is to compare the $R = 5, p = 1$ solution with a high-p solution obtained at a compatible cost, 27 s. This can be found for the $R = 2, p = 6$ solution which shows a drop of two orders of magnitude in the sea level error.

The data of Table IV and the trends shown in Figure 5 indicate several interesting features of h and p convergence when combined with a frontal solution algorithm. First note that an *a priori* estimate of the run time can be given as follows. Asymptotically the error can be expressed as $e \propto h^p$, while the run time can be expressed as $t_{solve} \propto Nw^2$, where N is the number of degrees of freedom in the problem and w is the RMS average frontwidth. N can be estimated as $N \propto p/h$, while w can also be estimated as $w \propto p/h$. This gives $t_{\text{solve}} \propto (p/h)^4$. Solving for the runtime as a function of the error level gives $t_{\text{solve}} = cp^4 e^{-4/p}$ with a constant of proportionality c. Taking logarithms yields $\ln(t) = -4p^{-1}\ln(e) + \ln(p^4) + c$. Hence, as p increases, there are two competing terms in the run time estimate. Increasing p from $p = 1$, and varying h such that the error level e is fixed, initially decreases the run time owing to the $4/p$ term. However, as p is further increased, the $\ln(p^4)$ term eventually becomes dominant and the run time increases. Thus one expects an optimal combination

Table IV. Shelf break hyperbolic tangent bathymetry: L^2 norm of error in depth-averaged velocity u as refinement level R and p vary· Frontal solver CPU times in seconds are shown in parentheses

	$R = 0$	$R = 1$	$R = 2$	$R = 3$	$R = 4$	$R = 5$
$p = 2$	7·605	2·284	0·349	0·856e-1	0·2123e-1	0·562e-2
	(0·12)	(0·19)	(0·40)	(1·25)	(5·05)	(27·43)
$p = 2$	3·074	0·672	0·670e-1	0·138e-1	0·321e-2	0·793e-3
	(0·11)	(0·20)	(0·58)	(2·47)	(15·86)	(192·64)
$p = 3$	1·295	0·112	0·966e-2	0·105e-2	0·123e-3	0·152e-4
	(0·17)	(0·41)	(1·49)	(7·54)	(67·98)	(854·09)
$p = 4$	0·416	0·111e-1	0·168e-2	0·705e-4	0·429e-5	—
	(0·35)	(1·08)	(4·28)	(22·62)	(206·91)	—
$p = 6$	0·354e-1	0·359e-2	0·239e-4	0·472e-6	—	—
	(1·20)	(4·27)	(18·01)	(113·00)	—	—
$p = 8$	0·248e-1	0·376e-3	0·402e-6	0·486e-8	—	—
	(4·29)	(15·59)	(68·90)	(362·40)	—	—

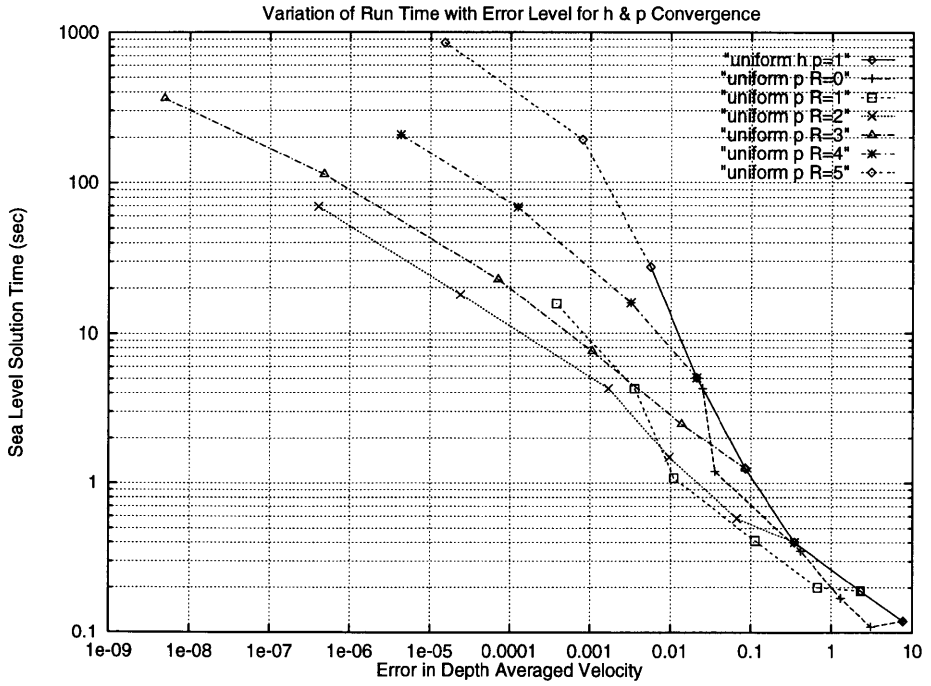

Figure 5. Shelf break hyperbolic tangent bathymetry: variation in run time with L^2 error in depth-averaged velocity for h and p refinement. The grids $R = 1, 2, 3, 4, 5$ are generated from grid $R = 0$ by uniform h refinement

of p and h that will minimize the run time for a given error tolerance. Examining the data of Table IV for $R = 4, p = 1$; $R = 3, p = 2$; $R = 2, p = 3$; $R = 1, p = 4$ and $R = 0, p = 8$ shows just such a behaviour. A minimum in the run time can be inferred near $R = 2, p = 3$ and $R = 1, p = 4$ The other data points shows a greater run time for a similar or greater error level. The results for this test problem indicate that pure p convergence from a coarse mesh is not desirable, nor is h-type convergence with low p. There is a clear minimal run time for moderate values of error in the depth-averaged velocity obtained for some amount of h refinement followed by moderate levels of p refinement.

The foregoing results then point to an effective strategy for obtaining both efficient and accurate solutions. First, a relatively coarse grid is created for the region of interest. Next, this grid is refined locally based on some error estimate until the geometry and problem data (such as bathymetry) are properly resolved and the errors are distributed uniformly. Finally, moderate levels of p refinement are applied to obtain an accurate solution. This strategy can be demonstrated for the shelf test case with hyperbolic tangent variation in depth. Starting with the 20-element grid (the grid in Figure 2, $p = 1, N = 17$), the elements are refined based on the element residual as an error estimate. For convenience the refinement is kept uniform in the y (along-shelf) direction and allowed to vary in the x (cross-shelf) direction (where the data vary). This produces a mesh ($p = 1, N = 31$) with clustering around the shelf break. Beyond this point, uniform p reinement is applied. The results for this procedure are summarized in Table V, which includes the number of nodes, N, the element order p and the L^2 norm of the error in both sea level and depth-averaged velocity. In following this strategy, the curve for run time versus error lies below all the other curves in Figure 5. This strategy differs from the previous one in that there is no optimal p as alluded to for the shelf break problem with

Table V. L^2 norm of error in sea level η and L^2 norm of error in depth-averaged velocity u using refinement strategies described in text (N, number of nodes; p, element order). Maximum frontwidth and solution time are also shown

N	p	$L^2\eta$	L^2u	FW	t
17	1	0·021652	2·288078	5	0·19
31	1	0·005631	0·325023	7	0·24
105	2	0·000192	0·064857	14	0·40
223	3	0·000041	0·012942	22	1·02
385	4	0·000029	0·003134	31	2·88
841	6	0·000028	0·000127	52	11·80
1473	8	0·000028	0·000003	77	42·05

uniform h refinements. Instead, one obtains a locally h-refined grid ($p = 1$) that will resolve solution features in areas of large gradients (in this case at the shelf break). One then applies uniform p refinement to achieve the desired solution error level.

In summary, the results for this problem demonstrate both the greater efficiencies obtainable with p refinement and some of the associated problems. For 1% error levels in the velocity solution, decreases in the solution time by an order of magnitude have been obtained. Conversely, the difficulties of dealing with highly variable bathymetry data over coarse element meshes have also been shown. Before considering the effects of domain geometry for a field-scale problem, the issues of equation (21) are revisited.

The results obtained for the shelf problem with piecewise linear variation in the bathymetry and equation (21) suggests that continuity errors can be reduced by interpolating $\mathbf{T}_n$ with a polynomial of degree $p-1$ when η is approximated by polynomials of degree p. Thus in equation (14) one uses the quantity $\hat{\mathbf{T}}_n$, which is constructed by computing $\bar{\mathbf{T}}_n$ as a function of degree p within each element and then degrading it by interpolation with a polynomial of degree $p-1$. Results for such strategy applied to the tanh shelf problem of Table V are shown in Table VI. Note that the continuity error, as reflected by the velocity error in column four, remains at round-off levels. Although the error in sea level only needs to be less than about 0·001 for an applied problem, the velocity errors obtained using full-order approximation of $\bar{\mathbf{T}}_n$ at such a sea level error are too large, as shown in Table V. However, if $\bar{\mathbf{T}}_n$ is interpolated at one degree less than the approximation for η, such that it is consistent with $\nabla\eta$ as noted earlier, then the velocity error, and hence continuity, is satisfied well as shown in Table VI. Thus acceptable solutions can be obtained at a much lower degree in p. Comparing the sea level error

Table VI. L^2 norm of error in sea level η and L^2 norm of error in depth-averaged velocity u (N, number of nodes; p, element degree). $\hat{\mathbf{T}}_n$ is used rather than $\bar{\mathbf{T}}_n$

N	p	$L^2\eta$	L^2u	$L_2\eta(21)$
17	1	0·021852	$O(10^{-13})$	***
31	1	0·005674	$O(10^{-13})$	0·006264
105	2	0·003061	$O(10^{-13})$	0·003683
223	3	0·000049	$O(10^{-13})$	0·000861
385	4	0·000028	$O(10^{-13})$	0·000878
841	6	0·000018	$O(10^{-13})$	0·000869
1473	8	0·000018	$O(10^{-13})$	0·000868

results for $p = 2$ and 3 in Tables V and VI shows that there is a loss of accuracy in the sea level solution when $\hat{\mathbf{T}}_n$ is used. However, this loss is minimal and provides enhanced continuity accuracy. It should be noted that in both Tables V and VI the sea level error stagnates at approximately 2×10^{-5}. This is due to insufficient resolution in the vertical (which gives poor resolution of the bottom boundary layer and hence bottom friction). The results of Tables V and VI were computed using 41 equispaced levels in the vertical, with the exception of the last column of Table VI where only 21 levels were used for comparison. Note that the sea level error for the 21-level solution stagnates at 8×10^{-4}. Examination of the vertical velocity profiles clearly showed problems in resolving the bottom boundary layer.

4.3. Field-scale problem

The San Juan Islands test case is a field-scale problem designed to test the methods developed in this paper in a highly irregular but realistic domain. The area chosen includes part of the inland marine waters that lie between the State of Washington, U.S.A. and the province of British Columbia, Canada. The area encompasses the inner part of the San Juan Islands (Figure 6) and is a subset of a larger grid for the entire boundary waters region.[32] The San Juan Islands grid is approximately 46 km in an east–west direction and 38 km in a north–south direction. The depth is held fixed at 100 m in order to focus on issues of domain irregularity. The basic grid contains 1715 nodes and 2246 elements that were formed using automatic grid generation methods.33 Two levels are used in the vertical with a linear bottom friction model. The calculations presented here are for the M_2 tidal constituent. The boundary conditions at the four open boundaries are interpolated from the larger model and the viscosity formulation is the same as used in the earlier work.

As opposed to the test cases with analytical solutions, it is more problematic to construct and interpret a measure of error for this field-scale case. The method chosen here involves computing a sequence of approximate solutions corresponding to uniform p refinement, essentially until memory is exhausted. The last such solution, corresponding to the highest p-value attainable within memory constraints, is used as a reference solution. The L^2 norms of the differences between this reference solution and the other solutions in the sequence are presented as indicators of the error.

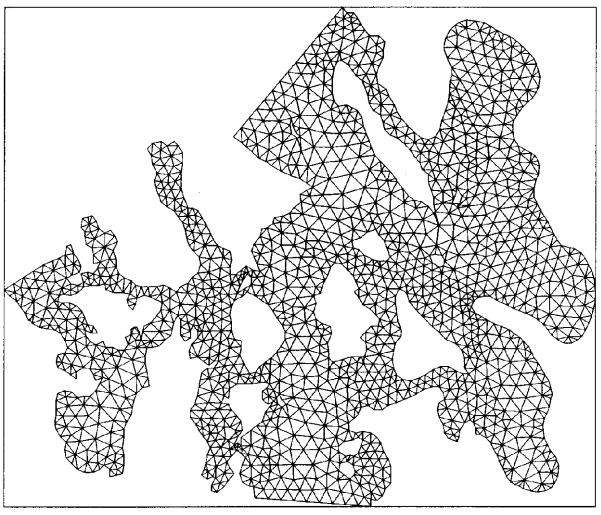

Figure 6. Grid for San Juan Island test case, initial grid R0

An initial uniform p refinement of the grid as shown in Figure 6 demonstrates poor convergence rates. Detailed examination of the differences between the solutions as p is increased indicates that the source of the problem is confined to small areas of the grid. Specifically, one finds that large currents generated around sharp headlands in the domain are responsible for singular behaviour in the solution on the boundary. These domain features generate r^{α}-type singularities, with α approaching $\frac{1}{2}$ as the interior angle on the boundary approaches 2π.

As noted in many previous studies,[19–21,34–37] pollution effects from singularities can be dealt with through a combination of adaptive h and p refinement. Figure 7 shows details of a subsection of the Figure 6 grid after four levels of successive adaptive h refinement. The refinement method used here is easy to implement. On each mesh level, uniform p refinement is applied as before. The L^2 norm of the difference between a reference solution ($p = 4$ or 6) and the $p = 1$ solution is computed for each element. All elements for which this error indicator exceeds a fixed level are refined. A 4:1-type refinement for triangles is used. Neighbouring elements are split to preserve a C^0 basis without resorting to inter-element constraints. Although this method is simple, it appears to work reasonably well. Many other choices have been explored in the literature, including truncation error methods[38]

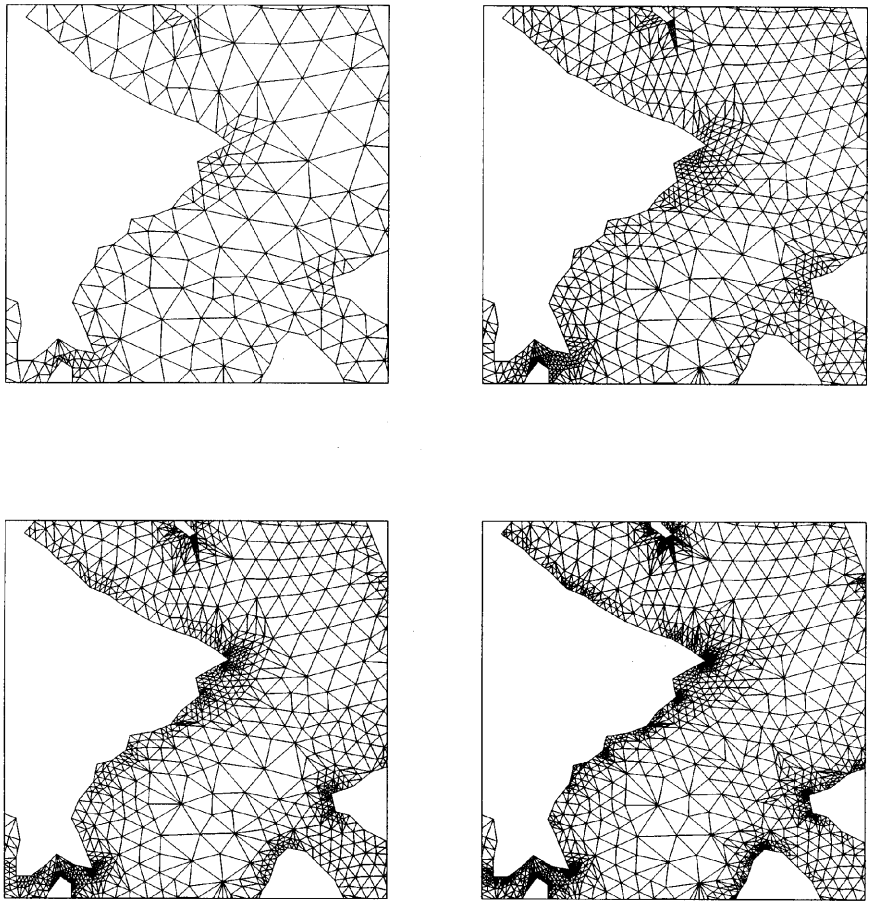

Figure 7. Details of San Juan Islands grid, refinements R1 (upper left), R2 (upper right), R3 (lower left) and R4 (lower right)

for shallow water problems. A survey of five methods is presented by Oden *et al.*,[39] where it is concluded that an element residual technique based on local enrichments is effective for a broad class of problems.

Figure 8 presents results for the five meshes of Figures 6 and 7, labelled R0, R1, R2, R3 and R4. Uniform p refinement is applied to each element mesh. Also shown are results for uniform h refinement. The results show that variation in the sea level error indicator in the L^2 norm as N, the number of degrees of freedom in the discretization, varies. The superiority of the h adaptive methods followed by p refinement when compared with the uniform h methods is clear. Although convergence is not exponential, the rates attained are quite good relatively speaking.

In order to run this problem with several levels of refinement, an iterative solution method was used running in parallel on a 32-node Intel Paragon. While these run times cannot be compared with those presented for the shelf break problem, they are internally consistent and provide a reasonable basis for comparison for this problem. Full details of the parallel implementation are beyond the scope of this study. Some details of the iterative method can be found in Reference 40. Figure 9 shows the variation in the solution time with error indicator level for the data points of Figure 8. It was observed that a sea level error of 10^{-5} roughly corresponds to a a1% relative error in velocity. At this error level, three combinations of adaptive refinement and p appear competitive: R1, $p=4$; R2, $p=3$ and R4, $p=2$ with observed run times of 88·2, 173·2 and 150·5 s respectively. In this case the preferred method appears to be moderate h refinement to isolate singularities on the boundary followed by p refinement to the desired error levels. However, this conclusion is susceptible to a number of factors. The R1 and R2 meshes are quite different in that R1 applies refinement only around the strongest of the singularities while R2 adds refinement around much of the boundary and in the interior. The issue then is one of obtaining an optimal distribution of h refinements. This and related problems have been considered in detail in a series of papers by Oden and co-

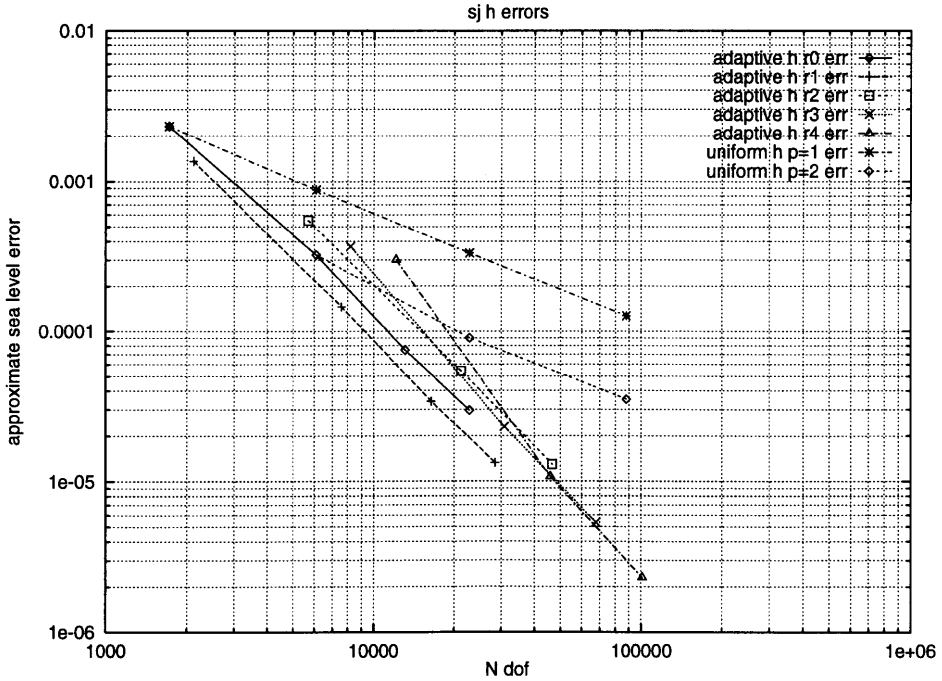

Figure 8. San Juan Islands: variation in approximate L^2 sea level error for h and p refinement

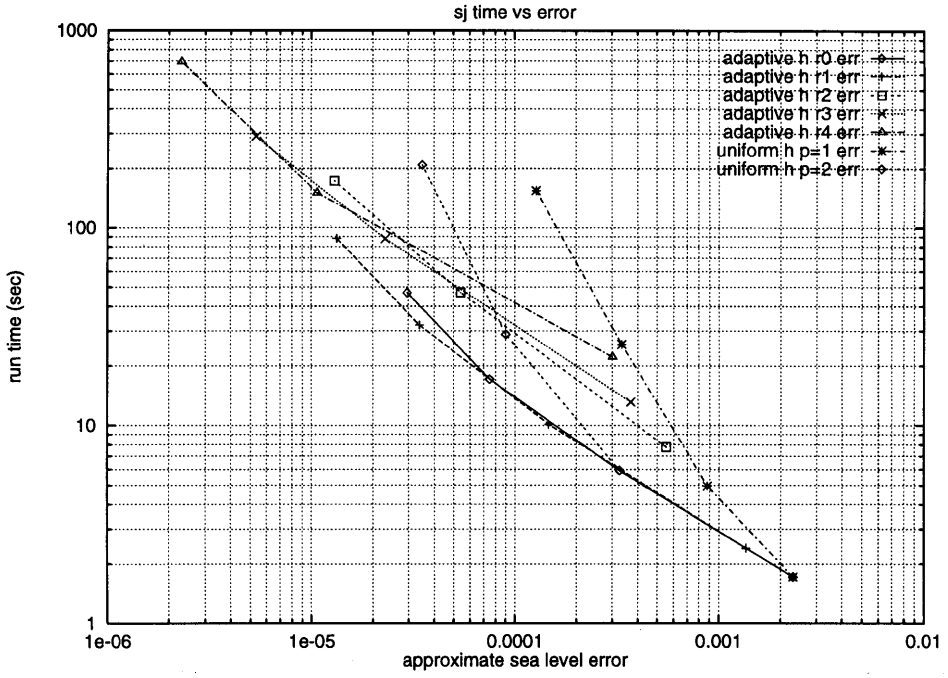

Figure 9. San Juan Islands: variation in run time with approximate L^2 sea level error

workers,[21,36,37,39,42] which has resulted in a method for obtaining optimal distributions of both local h and p refinements. Recent results by Oden and Patra[37] for this 'three-step method' appears to give exponential rates of convergence for model problems with $r^{2/3}$-type singularities while minimizing overall computational effort. The results for R4, $p = 2$ are interesting in that they provide good results at reasonable cost and are consistent with early results of Le Provost and Vincent.[15] In that study it was found that very efficient solutions for the wave equation form of the shallow water equations could be obtained with quadratic elements and graded meshes. Data presented there seem to indicate improved performance for cubic elements, although it is not as pronounced as the transition from linears to quadratics, and that the extra accuracy is not needed.

5. CONCLUSIONS

Using several test cases of varying computational difficulty, questions of accuracy and efficiency have been explored for uniform h and p refinement of finite element approximations to the shallow water equations. The results for the test cases show that high convergence rates can be obtained with uniform p refinement. For simple problem geometry, moderate levels of h and p refinement lead to the most efficient solutions. Improvements in solution efficiency of an order of magnitude have been observed when compared with uniform h refinement. For field-scale problems with complex geometry the wave equation formulation leads to solution singularities on the boundary. Uniform h or p refinement proves ineffective at resolving and controlling these local solution features. However, adaptive h refinement coupled with uniform p refinement appears to be effective in dealing with these problems. More sophisticated techniques, such as those in References 15, 20, 21, 37 and 38, may be worth the additional effort in implementation over the uniform p scheme used here, particularly for

coastal and estuarine problems with highly irregular geometries. The results of this study indicate that the possibility of adding p refinement to an existing h adaptive shallow water code or local h refinement to an existing p code should be considered.

Questions also arose in the treatment of bathymetry data. Here the issue is one of integrating field bathymetric data into the p solution scheme. For field data, one common scheme is to triangulate the bathymetric data to produce a piecewise linear approximation. These data can then be interpolated to the computational grid. However, problems can arise for the p scheme when these data are interpolated at high p-values. This was demonstrated with the second test problem involving a hyperbolic tangent variation in the bathymetry. Further study of this issue is required in the content of adaptive h refinement, where the adaptive refinement procedure may resolve some of these interpolation problems.

Finally, questions about the choice of approximation spaces for sea level and velocity have arisen. These are particularly important in the context of p refinement. The approach taken here is to approximate η by polynomials of degree p, while $\mathbf{T}$ in (14) is approximated by polynomials of degree $p-1$. Results for the continental shelf test case support this approach and the notion that there is a consistency requirement for the approximation of $\nabla\eta$ and $\mathbf{T}$. The resulting solutions show both accurate velocity and continuity at the expense of minor degradation in the sea level accuracy as compared with the same-order approximation. This accuracy is recovered with additional p refinement.

ACKNOWLEDGEMENTS

The authors would like to acknowledge the many helpful comments of Graham Carey and Johannes Westerink during the course of this work. This work was funded by the National Research Program of the U.S. Geological Survey.

REFERENCES

1. C. E. Pearson and D. F. Winter, 'On the calculation of tidal currents in homogeneous estuaries', *J. Phys. Oceanogr.*, **7**, 520 (1977).
2. R. L. Snyder, M. Sidjabat and J. H. Filloux, 'A study of tides, setup, and bottom friction in a shallow semi-enclosed basin. Part II: Tidal model and comparison with data', *J. Phys. Oceanogr.*, **9**, 170–188 (1979).
3. D. R. Lynch and W. G. Gray, 'A wave equation model for finite element tidal computations', *Comput. Fluids*, **7**, 207–228 (1979).
4. C. Le Provost, G. Rougier and A. Poncet, 'Numerical modelling of the harmonic constituents of the tides, with application to the English Channel', *J. Phys. Oceanogr.*, **11**, 1123–1138 (1981).
5. M. Kawahara and K. Hasegawa, 'Periodic Galerkin finite element method of tidal flow', *Int. j. numer methods eng.*, **12**, 115 (1978).
6. D. R. Lynch and F. E. Werner, 'Three dimensional hydrodynamics on finite elements. Part 1: Linearized harmonic model', *Int. j. numer. methods fluids*, **7**, 871–909 (1987).
7. D. R. Lynch and F. E. Werner, 'Three dimensional hydrodynamics on finite elements. Part 2: Nonlinear time stepping model', *Int. j. numer methods fluids*, **12**, 507–533 (1991).
8. R. A. Walters, 'A model for tides and currents in the English Channel and southern North Sea', *Adv. Water Res.*, **10**, 138–148 (1987).
9. R. A. Walters, 'A three-dimensional, finite element model for coastal and estuarine circulation', *Continental Shelf Res.*, **12**, 83–102 (1992).
10. R. A. Walters and M. G. G. Foreman, 'A three-dimensional, finite element model for baroclinic circulation on the Vancouver Island continental shelf', *J. Marine Syst.*, **3**, 507–518 (1992).
11. J. J. Westerink, J. J. Conner and K. D. Stolzenbach, 'A primitive pseudo wave equation formulation for solving the harmonic shallow water equations', *Adv. Water Res.*, **10**, 188–199 (1987).
12. J. J. Westerink and W. G. Gray, 'Progress in surface water modelling', *Rev. Geophys., Suppl.*, April, 201–217 (1991).
13. R. A. Walters and R. T. Chen, 'Accuracy of an estuarine hydrodynamic model using smooth elements', *Water Resources Res.*, **16**, 187–195 (1980).

14. R. A. Walters, 'Numerically induced oscillations in finite element approximations to the shallow water equations', *Int. j. numer. methods fluids*, **3**, 591–604 (1983).
15. C. Le Provost and P. Vincent, 'Some tests of precision for a finite element model of ocean tides', *J. Comput. Phys.*, **65**, 273–291 (1986).
16. E. Becker, G. F. Carey and J. T. Oden, *Finite Elements: An Introduction*, Prentice-Hall, Englewood Cliffs, NJ, 1981.
17. I. Babuska, B. A. Szabo and I. N. Katz, 'The *p*-version of the finite element method', *SIAM J. Numer. And.*, **18**, 515–544 (1981).
18. I. Babuska and B. Guo, 'The p version of the finite element method for domains with curved boundaries', *SIAM J. Numer. Anal.*, **25**, 837–861 (1988).
19. I. Babuska and M. Suri, 'the h–p version of the finite element method with quasiuniform meshes', *Math. Mod. Numer. Anal.*, **21**, 199–238 (1987).
20. J. T. Oden and L. Demkowicz, '*hp* adaptive finite element methods in computational fluid dynamics', *Comput. Methods Appl. Mech. Eng.*, **89**, 11–40 (1991).
21. J. T. Oden, W. Wu and V. Legat, 'An *hp* adaptive strategy for finite element approximations of the Navier–Stokes equations', *Int. j. numer. methods fluids*, **20**, 831–851 (1995).
22. L. Demkowicz, J. T. Oden and W. Rachowicz, 'A new finite element method for solving compressible Navier–Stokes equations based on an operator splitting method and *hp* adaptivity', *Comput. Methods Appl. Mech. Eng.*, **84**, 275–326 (1990).
23. L. Demokowicz, J. T. Oden, W. Rachowicz and O. Hardy, 'An *hp* Taylor–Galerkin finite element method for compressible Euler equations', *Comput. Methods Appl. Mech. Eng.*, **88**, 363–396 (1991).
24. A. T. Patera, 'A spectral element method for fluid dynamics; laminar flow in a channel expansion', *J. Comput. Phys.*, **54**, 468–477 (1984).
25. Y. Maday and A. Quarteroni, 'Spectral and pseudo spectral approximations of the Navier Stokes equations', *SIAM J. Numer. Anal.*, **19**, 761–780 (1982).
26. P. Fischer and E. Ronquist, 'Spectral element method for large scale parallel Navier–Stokes calculations', Comput. Methods Appl. Mech. Eng., **116**, 69–76 (1994).
27. M. Iskandarani, D. Haidvogel and J. Boyd, 'A staggered spectral element model with application to the oceanic shallow water equations', *Int. j. numer. methods fluids*, **20**, 393–414 (1995).
28. H. Ma, 'A spectral element basin model for the shallow water equations', *J. Comput. Phys.*, **109**, 133–149 (1993).
29. R. A. Walters, 'A model study of tidal and residual circulation in Delaware Bay and River', *J. Geophys. Res.*, in press.
30. R. L. Haney, On the pressure gradient force over steep topography in sigma coordinate ocean models', *J. Phys. Oceanogr.*, **21**, 610–619 (1991).
31. C. B. Officer, *Physical Oceanography of Estuaries (and Associated Coastal Waters)*, Wiley, New York, 1976.
32. M. G. G. Foreman, R. A. Walters, R. F. Henry, C. P. Keller and A. G. Dolling, 'A tidal model for eastern Juan de Fuca Strait and the southern Strait of Georgie', *J. Geophys. Res.*, **100**(C1), 721–740 (1995).
33. R. F. Henry and R. A. Walters, 'A geometrically-based, automatic generator for irregular triangular networks', *Commun. Numer. Methods Eng.*, **9**, 555–566 (1993).
34. I. Babuska and B. Guo, 'The h, p, h–p version of FEM for 1-d problem: 1 p error analysis, II h, h–p error analysis, III Adaptive h–p', *Numer. Math.*, **49**, 577–683 (1986).
35. I. Babuska and B. Guo, 'h–p version FEM: I Basic approximation results, II General results', *Comput. Mech.*, **1**, 21–45 (1986).
36. W. Rachowicz, J. T. Oden and L. Demkowicz, 'Toward a universal *hp* adaptive finite element strategy, Part 3. Design of *hp* meshes', Comput. Methods Appl. Mech. Eng., **77**, 181–212 (1989).
37. J. T. Oden and A. Patra, 'A parallel adaptive stategy for *hp* finite element computations', *Comput. Methods Appl. Mech. Eng.*, **121**, 449–470 (1995).
38. J. J. Westerink and P. J. Roache, 'Issues in convergence studies in geophysical flow computations', in *Quantification of Uncertainty in Computational Fluid Dynamics*, FED Vol. 213, ASME, New York, 1995.
39. J. T. Oden, L. Demkowicz, W. Rachowicz and T. Westerman, 'Toward a universal *hp* adaptive finite element strategy, Part 2. A posterio error estimation', *Comput. Methods Appl. Mech. Eng.*, **77**, 113–180 (1989).
40. E. Barragy, G. Carey and R. Walters, 'Application of conjugate gradient methods to tidal simulation', *Adv. Water Res.*, **16**, 163–171 (1993).
41. L. Demkowicz, J. T. Oden, W. Rachowicz and O. Hardy, 'Towards a universal *hp* adaptive finite element strategy, Part 1. Constrained approximation and data structure', **77**, 79–112 (1989).